# Dynamic behavior of Josephson-coupled layered structures

R. Kleiner and P. Müller
*Walther-Meissner-Institut, D-85748 Garching, Germany*

H. Kohlstedt
*Institut für Schicht-und Ionentechnik, Forschungszentrum Jülich, D-52425 Jülich, Germany*

N. F. Pedersen
*Physical Laboratory I, Technical University of Denmark, DK-2800 Lyngby, Denmark*

S. Sakai
*Electrotechnical Laboratory, 1-1-4 Umezono, Tsukuba-shi, Ibaraki 305, Japan*
(Received 13 January 1994)

We have investigated Josephson effects in stacks of both artificial and natural Josephson junctions. The measurements have been performed on Nb/Al-$AlO_x$/Nb multilayers and on small single crystals of $Bi_2Sr_2CaCu_2O_8$. Both systems exhibit multiple branched $I$-$V$ characteristics in zero magnetic field. In finite magnetic fields coupling via currents flowing along the superconducting layers is essential, since the layers are thinner than the London penetration depth. All observations are in good agreement with numerical simulations of stacks of coupled Josephson junctions. These simulations predict that a large number of junctions can be phase locked in large magnetic fields via Fiske resonances excited in all junctions.

## I. INTRODUCTION

Many applications of the Josephson effect, such as submillimeter sources, detectors, or mixers, are intimately connected with the use of large arrays of interacting Josephson tunnel junctions.[1] Planar arrays of thousands of junctions can be fabricated relatively easy in niobium technology.[2] However, the lateral dimensions of these arrays soon exceed the wavelength in high-frequency applications, which severely restricts at least the tunability of such devices. In order to avoid such restrictions, vertical packaging of junctions is necessary. Stacks of Josephson junctions, however, differ qualitatively from planar structures. First of all, the thickness of the superconducting layers (the electrodes) is comparable or even much smaller than the London penetration depth $\lambda$. Screening currents in magnetic fields or transport currents flowing along the superconducting layers will spread over a distance $\lambda$, thus coupling the stacked junctions. Second, transport currents flowing perpendicular to the layers will weaken the order parameter at the superconductor-insulator interface within one Ginzburg-Landau coherence length $\xi$. If the electrode thickness is comparable or smaller than $\xi$, this mechanism couples adjacent Josephson junctions.[3] Third, in the resistive state the transport current is partly carried by quasiparticles which diffuse into the electrodes on the length scale of the quasiparticle diffusion length $\Lambda_q$, which can be several micrometers.[3] If the electrode thicknesses are less than $\Lambda_q$, a junction being in the resistive state increases the subgap conductivity and decreases the gap voltage in the adjacent junction. At least, this nonequilibrium injection of quasiparticles should be an effective coupling mechanism in stacked Josephson junctions. In contrast, the electromagnetic interaction, which is regarded as the most important coupling mechanism in planar arrays, may only play a minor role in vertical structures. Electromagnetic coupling originates from ac Josephson currents flowing in a resistive state, thus creating electromagnetic radiation. This radiation can be absorbed by other junctions, thus providing a long-range coupling mechanism. However, there is no radiation in the direction of current flow and therefore this mechanism is probably not effective in vertical structures.

Whereas electromagnetic coupling has been studied intensively, little is known about all other mechanisms. Therefore the purpose of this paper is an experimental and theoretical comparison of Josephson effects in stacked Josephson tunnel junctions made from very different materials, namely, artificially fabricated Nb/Al-$AlO_x$/Nb multilayers[4] and single crystals of the high-$T_c$ superconductor $Bi_2Sr_2CaCu_2O_{8+x}$ (BSCCO). The latter forms natural stacks of Josephson junctions with the $CuO_2$ layers acting as superconducting electrodes and the $Bi_2O_3$ layers acting as insulating barrier ("intrinsic Josephson effect"; cf. Fig. 1).[5] We compare all experimental results with numerical calculations using coupled sine-Gordon equations.[6–8]

The paper is organized as follows.

In Sec. II we introduce the basic model of stacked Josephson junctions in order to discuss relevant time and length scales quantitatively. Additionally, we present numerical solutions for a stack of five junctions. In Sec. III materials are characterized and measuring techniques are described. The results (Sec. IV) are separated into a discussion of the current-voltage characteristics in zero field and the magnetic field dependence of the critical current.

0163-1829/94/50(6)/3942(11)/$06.00  

## II. BASIC CONCEPTS

### A. Sine-Gordon equation

In the following we want to describe briefly the electrodynamics of a stack of $N$ Josephson junctions (Fig. 2). A detailed discussion in a slightly different notation can be found in the paper by Sakai, Bodin, and Pedersen.[6] The stack consists of $N+1$ superconducting electrodes of thickness $d_n$ separated by $N$ insulating layers of thickness $t_n$. The length of the stack in the $x$ direction is $b$; its width in the $y$ direction is $a$. The width $a$ is assumed to be small compared to the characteristic lengths $\lambda_m$ and $\lambda_k$ introduced later. An external magnetic field $H$ is applied along $y$. The bias current $j_{\rm ext}$ is fed homogeneously into the outermost electrodes labeled 0 and $N$. The phase of the order parameter in the $n$th electrode is $\varphi_n$. The densities of the Josephson currents $j_{zn}$ flowing in the $z$ direction across the $n$th Josephson junction within the stack are described by the two Josephson equations

$$j_{zn}=j_c\sin(\gamma_n)\ , \tag{1}$$

$$\hbar\dot{\gamma}_n=2et_nE_{zn}\ , \tag{2}$$

where

$$\gamma_n=\varphi_n-\varphi_{n-1}-\frac{2e}{\hbar}\int_{(n-1)(t+d)}^{n(t+d)}A_z dz$$

is the gauge-invariant phase difference of the order parameter in the electrodes of the $n$th junction. $E_{zn}$ is the electric field across the $n$th junction.

If variations of the amplitude of the order parameter inside the electrodes can be neglected and the gradient of $\varphi_n$ along $y$ is negligible in the superconducting layers, the gradient along $x$ of $\varphi_n$ is given by

$$\varphi_n'\equiv\frac{d\varphi_n}{dx}=\frac{2e}{\hbar}(A_{x,n}+\mu_0\lambda^2 j_{x,n})\ . \tag{3}$$

Here $j_{x,n}$ denotes the supercurrents flowing along the $n$th electrode, and $A_{x,n}$ is the $x$ component of the vector potential. $\lambda$ is the London penetration depth for screening currents flowing in the $xy$ direction.

For the $z$ dependence of the magnetic field inside the $n$th electrode, we use the symmetrized form

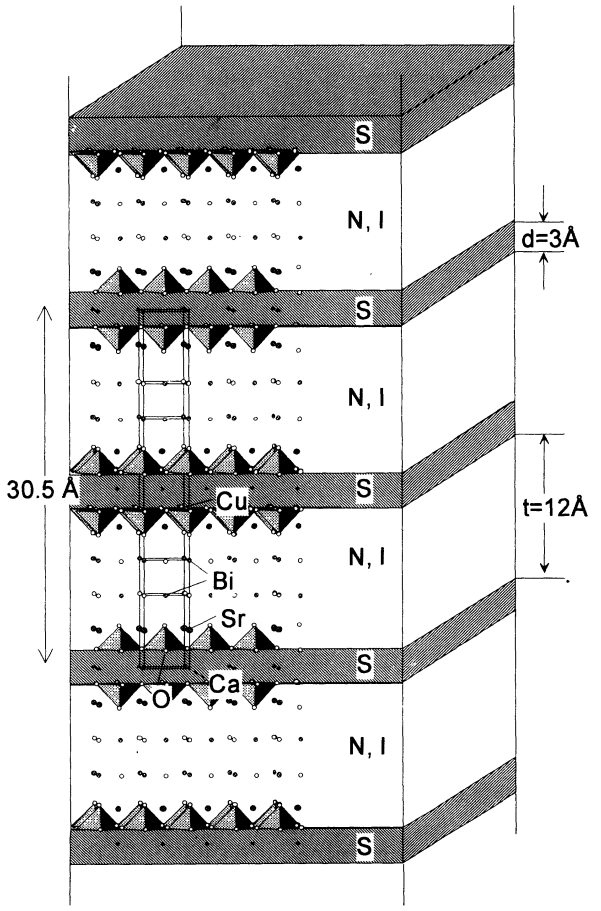


FIG. 1. Superposition of the crystal structure of BSCCO and the model of stacked intrinsic Josephson junctions. $S$, superconducting $CuO_2$ bilayer; $N,I$, normal or insulating layer consisting of $Bi_2O_3$ and SrO.

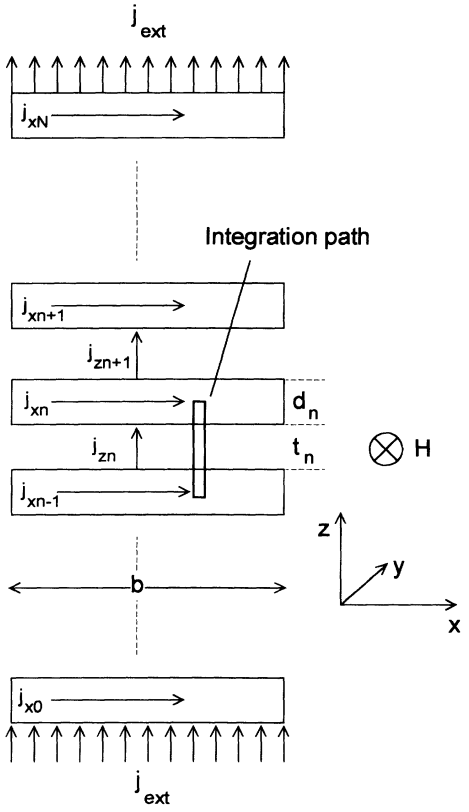


FIG. 2. Stack of $N$ Josephson junctions in a magnetic field. The electrodes are numbered from 0 to $N$. The thickness of the $n$th superconducting electrode is $d_n$. The thickness of the $n$th barrier located between the electrodes $n-1$ and $n$ is $t_n$. The width of the stack in the $x$ direction is $b$. Screening currents flowing along the $n$th electrode are denoted $j_{xn}$. $z$-axis currents flowing across the $n$th Josephson junctions of the stack are denoted $j_{zn}$. Transport currents with homogeneous density $j_{\rm ext}$ are fed into the outermost electrodes Nos. 0 and $N$. The external magnetic field is directed along $y$ perpendicular to the layers. The integration path (thick line) is used to obtain Eq. (4).

$$\frac{H_n+H_{n+1}}{2}\frac{\cosh(z/\lambda)}{\cosh(d_n/2\lambda)}+\frac{H_{n+1}-H_n}{2}\frac{\sinh(z/\lambda)}{\sinh(d_n/2\lambda)} .$$

$H_n$ is the $y$ component of the magnetic field in the $n$th barrier. For the sake of simplicity, for the following analysis, we assume that all junction parameters are identical. Integrating (3) along the line shown in Fig. 2 and taking the derivative in the $x$ direction yields

$$\gamma_n''=\frac{d^2\gamma_n}{dx^2}=\left[\frac{1}{\lambda_m^2}+\frac{2}{\lambda_k^2}\right]j_{z,n}-\frac{1}{\lambda_k^2}(j_{z,n-1}+j_{z,n+1}) -\frac{1}{\lambda_m^2}j_{\rm ext} , \tag{4}$$

$$\lambda_k=\left[\frac{\Phi_0 d_{\rm eff}}{2\pi\mu_0\lambda^2 j_c}\right]^{1/2} , \quad \lambda_m=\left[\frac{\Phi_0}{2\pi\mu_0 t_{\rm eff} j_c}\right]^{1/2} .$$

Here

$$d_{\rm eff}=\lambda\sinh(d/\lambda) ,$$

$$t_{\rm eff}=t+\lambda\tanh(d/2\lambda)+\lambda\tanh(d/2\lambda) ,$$

$$n=1,\ldots,N ,$$

and $j_c$ is the maximum density of the Josephson currents.

The $z$-axis currents $j_{z,n}$ are given by the sum of Josephson, Ohmic, and displacement currents, which may be expressed as

$$j_{z,n}=j_c\sin\gamma_n+\sigma E_{z,n}+\epsilon\epsilon_0\dot{E}_{z,n} =j_c\sin\gamma_n+\sigma\frac{\Phi_0}{2\pi t}\dot{\gamma}_n+\epsilon\epsilon_0\frac{\Phi_0}{2\pi t}\ddot{\gamma}_n . \tag{5}$$

Here $\sigma$ is the electric conductivity, $\epsilon$ is the dielectric constant, and $E_{z,n}$ is the electric field component in the $z$ direction across the $n$th barrier.

Bias currents are introduced by

$$j_{z,0}=j_{z,N+1}=j_{\rm ext} . \tag{6}$$

Additional boundary conditions are

$$\gamma_n'(x=0)=\gamma_n'(x=b)=\frac{2\pi\mu_0 t_{\rm eff}}{\Phi_0}H_{\rm ext} . \tag{7}$$

Equation (4) is the analog of the sine-Gordon equation describing the dynamics of single Josephson junctions. It obviously couples adjacent junctions within the stack. Defining a Josephson penetration depth

$$\lambda_j=\left[\frac{1}{\lambda_m^2}+\frac{2}{\lambda_k^2}\right]^{1/2} , \tag{8}$$

we can introduce a dimensionless coupling parameter by $s=(\lambda_j/\lambda_k)^2$. For electrode thicknesses much larger than $\lambda$, $s$ goes to zero, and in the opposite limit, $s$ approaches 0.5.

### B. Characteristic scales

If only a sufficiently small magnetic field is applied along $y$, at $j_{\rm ext}=0$, the phases $\gamma_n$ will be almost equal. Then Eq. (4) reduces to

$$\gamma_n''=\frac{1}{\lambda_m^2}j_{z,n}=\frac{1}{\lambda_m^2}\sin\gamma_n\approx\frac{1}{\lambda_m^2}\gamma_n . \tag{9}$$

In this sense $\lambda_m$ can be identified as the screening length for small magnetic fields directed along $y$. On the other hand, if there is a vortex in the $n$th junction, the current $j_{zn}$ approaches $j_c$ at some distance of the vortex core. The relevant length for this case is $\lambda_j$.

If the electrodes are much thicker than $\lambda$, the length $\lambda_k$ goes to infinity, and $\lambda_m,\lambda_j$ approach the standard expression for the Josephson penetration length,

$$\lambda_j=\left[\frac{\Phi_0}{2\pi\mu_0(\lambda+t)j_c}\right]^{1/2} . \tag{10}$$

In this limit Eq. (4) simply describes the dynamics of $N$ independent Josephson junctions. Defining a characteristic velocity $\bar{c}$ by

$$\frac{1}{\bar{c}^2}=\frac{1}{\bar{c}_m^2}+\frac{2}{\bar{c}_k^2} , \tag{11}$$

with

$$\frac{1}{\bar{c}_m^2}=\epsilon\epsilon_0\frac{\Phi_0}{2\pi t j_c}\frac{1}{\lambda_m^2} ,$$

$$\frac{1}{\bar{c}_k^2}=\epsilon\epsilon_0\frac{\Phi_0}{2\pi t j_c}\frac{1}{\lambda_k^2} ,$$

we find that, in the thick electrode limit, $\bar{c}$ approaches the standard Swihart velocity,

$$\bar{c}=\frac{c}{\sqrt{\epsilon}}\left[\frac{t}{2\lambda+t}\right]^{1/2} .$$

In the opposite case ($d\ll\lambda$), $\lambda_m$, $\lambda_k$, and $\lambda_j$ are given by

$$\lambda_m=\left[\frac{\Phi_0}{2\pi\mu_0(d+t)j_c}\right]^{1/2} ,$$

$$\lambda_k\approx\left[\frac{\Phi_0 d}{2\pi\mu_0\lambda^2 j_c}\right]^{1/2}=\frac{\lambda_m}{\lambda}\sqrt{d(t+d)} ,$$

$$\lambda_j=\left[\frac{\Phi_0}{2\pi\mu_0(\lambda^2/d+t+d)j_c}\right]^{1/2}\approx\lambda_k .$$

For the velocities $\bar{c}$, $\bar{c}_m$, and $\bar{c}_k$, we get

$$\bar{c}_m=\frac{c}{\sqrt{\epsilon}}\left[\frac{t}{t+d}\right]^{1/2} , \quad \bar{c}_k=\frac{c}{\sqrt{\epsilon}}\frac{\sqrt{dt}}{\lambda} , \quad \bar{c}=\frac{c}{\sqrt{\epsilon}}\frac{\sqrt{dt}}{\sqrt{2\lambda}} .$$

For BSCCO, the thickness of a $CuO_2$ bilayer is $d=3$ Å. The spacing between different bilayers is $t=12$ Å, and the zero-temperature penetration depth in the $ab$ direction is $\lambda(0)=1700$ Å. Critical current densities can be varied between 100 and 7000 A/cm$^2$ (cf. Sec. III). Taking $\epsilon=10$ as a guess yields $\bar{c}=10^{-3}c$. $\lambda_m$ ranges between 50 and 400 $\mu$m and $\lambda_k$ is less than 2 $\mu$m, and the coupling parameter $s$ is close to 0.5. The BSCCO crystals measured had lateral dimensions $a,b$ between 30 and 80 $\mu$m,

i.e., $\lambda_k \ll a,b \ll \lambda_m$. We note that in this case the condition $a < \lambda_k$ is not valid. We thus may have strong variations of the current density in the $y$ direction. Nevertheless, the one-dimensional model should be sufficient for the basic properties of the crystals, since screening and self-field effects occur on scales $\lambda_m$ and spatial variations induced by the external magnetic field occur perpendicular to $H_{\rm ext}$. For Nb/Al-AlO$_x$/Nb, the thickness of the inner Nb layers is 35 nm. The thickness of the Al-AlO$_x$ layer is 8 nm. Taking the thickness of the insulating AlO$_x$ barrier as $t=2$ nm yields a thickness of $d=41$ nm for the inner electrodes. For the outermost electrodes, $d=100$ and 280 nm, respectively. Other parameters are $\lambda=90$ nm, $j_c=250$ A/cm,$^2$ and $\epsilon=6$, which yields $\bar{c}=0.04c$, $\lambda_m=49.2$ $\mu$m, and $\lambda_k=23.7$ $\mu$m for the inner junctions and $\lambda_m=39$ $\mu$m, $\lambda_k=39.7$ $\mu$m and $\lambda_m=32$ $\mu$m, $\lambda_k=114$ $\mu$m for the outer ones. For the inner junctions, the coupling parameter $s=0.48$.

The Nb/Al-AlO$_x$/Nb stacks measured (see Fig. 3) had lateral dimensions of $20\times20$ $\mu$m,$^2$ which is less than $\lambda_m$ and $\lambda_k$. Thus they may be regarded as stacks of short Josephson junctions. Long stacked all-Nb tunnel junctions were investigated by Ustinov *et al.*[9] In addition, the problem of coupled long junction oscillators was discussed by Grønbech-Jensen and Blackburn.[9] Very recently, work on Fiske modes of grain boundary junctions in high-$T_c$ superconductors was published by Winkler.[9]

In the limit $a,b \ll \lambda_k,\lambda_m$, an integration of Eq. (4) leads to the well-known Fraunhofer pattern for the field dependence of the critical current of each junction:

$$I_{c,n}(H)=I_{c,n}(0)\left|\frac{\sin x}{x}\right| , \tag{12}$$

$$x=\pi\frac{H}{H_0} , \quad H_0=\frac{\Phi_0}{\mu_0 b t_{{\rm eff},n}} . \tag{13}$$

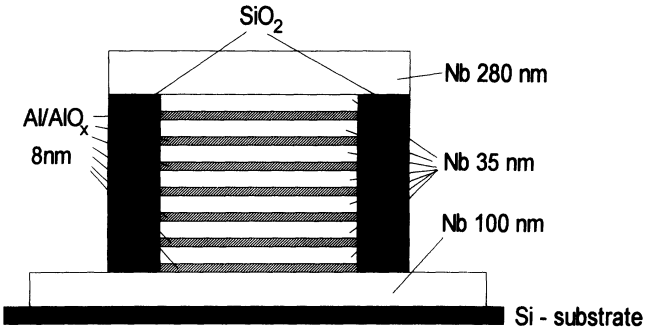


FIG. 3. Schematic view of the stack of seven Nb/Al-AlO$_x$/Nb junctions.

For the inner junctions of the Nb/Al-AlO$_x$/Nb stacks, we therefore expect the first zero of the Fraunhofer pattern at $H_0=24$ Oe; for the outer junctions, we get $H_0=10$ and 14 Oe.

For a BSCCO crystal with lateral dimensions of 1 $\mu$m, we would expect the first zero of the Fraunhofer pattern at a field of 1.4 T. Even for the crystal dimensions used, $H_0$ ranges between 170 and 450 Oe, which is comparable to $H_{c1}$ perpendicular to the electrodes. In order to avoid current inhomogeneities due to Abrikosov vortices in the electrodes, the $CuO_2$ planes have to be aligned perfectly with the external magnetic field.

### C. Special solutions

In order to convert the partial differential Eq. (4) to a set of ordinary differential equations, we use the multimode expansion introduced in Ref. 10.

For the phases $\gamma_n(x,t)$, we use the expressions

$$\begin{aligned}\gamma_n(x,t)&=\gamma_{n,0}(t)+\frac{2\pi\mu_0 t_{{\rm eff},n}H_{\rm ext}}{\Phi_0}x-\frac{2\pi}{\Phi_0}\mu_0\lambda^2\frac{b}{\pi}\sum_{k=1}^{K}\left[\frac{1}{k}[j_{n,k}(t)-j_{n-l,k}(t)]\cos\left[\pi k\frac{x}{b}\right]\right]\\&=\gamma_{n,0}(t)+2\pi\frac{H_{\rm ext}}{H_0}\frac{x}{b}-\sum_{k=1}^{K}\left[\gamma_{n,k}\cos\left[\pi k\frac{x}{b}\right]\right] .\end{aligned} \tag{14}$$

$\sin[\gamma_n(x,t)]$ can be expanded into a Fourier series as well:

$$\sin[\gamma_n(x,t)]=\sum_{k=0}^{K}\left[s_{n,k}\cos\left[\pi k\frac{x}{b}\right]\right] ,$$

$$s_{n,0}=\frac{1}{b}\int_0^b\sin[\gamma_n(x,t)]dx , \tag{15}$$

$$s_{n,k}=\frac{2}{b}\int_0^b\sin[\gamma_n(x,t)]\cos\left[\pi k\frac{x}{b}\right]dx ,$$

$$k=1,\ldots,K .$$

Substituting Eqs. (14) and (15) into Eq. (4) then yields a set of ordinary differential equations for the Fourier components $\gamma_{n,k}$, which can be solved by standard methods. For the simulations presented, we used between 10 and 20 Fourier components.

In the following we present solutions of a stack of $N=5$ junctions. The width of the junctions is 20 $\mu$m. We use $\lambda=1700$ Å and $j_c=150$ A/cm,$^2$ which are typical values for BSCCO. This yields $\lambda_m\approx341$ $\mu$m, $\lambda_k\approx1.52$ $\mu$m, and $\lambda_j\approx1.08$ $\mu$m. For the McCumber parameter

$$\beta_c=2\pi I_c R^2 C/\Phi_0=2\pi\epsilon\epsilon_0 j_c t/(\sigma^2\Phi_0) ,$$

we used $\beta_c=20$. Figure 4 shows a static solution with a single fluxon located in the middle junction. As can be

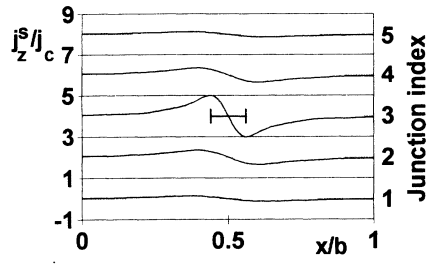


FIG. 4. One vortex solution for a stack of five junctions at zero field and zero external current. In order to show the spatial dependence of the Josephson currents of all junctions, we plot the supercurrent densities perpendicular to the layers, $j_{zn}^s = j_{cn}\sin(\gamma)$, vs the coordinate $x$ along the length $b$. Simulating the geometry of the stack, the curves of the single junctions are vertically offset. The total length of the stack is 20 $\mu$m, and $\lambda_m = 314$ $\mu$m. The length of the bar in the center of the middle junction equals $2\lambda_j = 2.2$ $\mu$m.

seen clearly, the fluxon induces Josephson currents in all junctions. Similar solutions have been discussed in Refs. 6 and 11. If we now put several fluxons into the stack, the vortices tend to form a triangular lattice as predicted in Ref. 12; i.e., the interaction between the vortices is repulsive (Fig. 5). Correspondingly, the interaction for vortex-antivortex pairs located in different junctions is attractive. In Fig. 6 we have calculated a static situation with a vortex-antivortex pair in each junction. We note that such a situation is not stable for a single vortex-antivortex pair since it tends to annihilate. However, in the configuration shown in Fig. 6, the repulsive vortex-vortex (or antivortex-antivortex) interaction cancels the attractive interaction of the vortex-antivortex pair in each layer. In fact, if the vortices are slightly displaced along $x$ during the simulation, they return to the stable position shown in Fig. 6.

The above solutions have been obtained by placing a certain number of fluxons into the system by choosing appropriate initial values $\gamma_{n,k}(t=0)$ for fixed $H_{\rm ext}$ and $j_{\rm ext}$. In contrast, in the simulations shown in Fig. 7 we started with a vortex-free state at $j_{\rm ext}=0$, $H_{\rm ext}=0$ and increased $H_{\rm ext}$ continuously. In this case we find a diamagnetic response up to $H_{\rm ext}=1.5H_0$ [Fig. 7(a)]. However, it

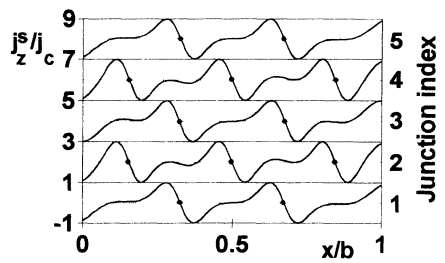


FIG. 5. Simulation of a stack of 5 junctions containing 12 vortices. $H_{\rm ext}=3H_0$, $j_{\rm ext}=0$. Points show the locations of the center of mass of the fluxons.

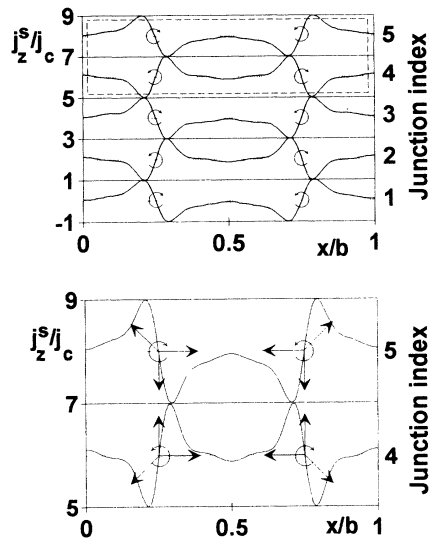


FIG. 6. Simulation of a stack of five junctions containing a vortex-antivortex pair in each layer (upper part). $H_{\rm ext}=j_{\rm ext}=0$. Circular arrows show the vorticity. Junctions Nos. 4 and 5 (dashed rectangle) are enlarged in the lower part of the figure. The straight arrows denote the balance of the forces acting on each of the vortices.

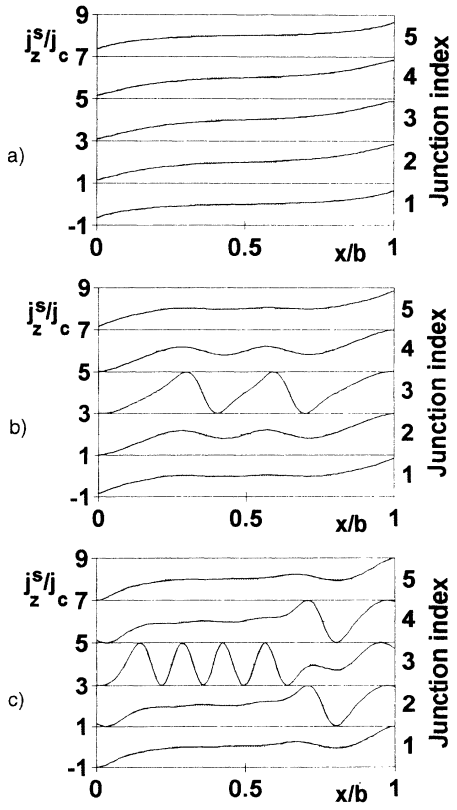


FIG. 7. Simulation of a stack of five junctions with zero external current. In the simulation, the magnetic field was increased continuously. The results are shown for three different values of the external field. For $H < 1.5H_0$ we find a diamagnetic response [(a) $H=H_0$]. At higher fields vortices penetrate the stack starting with the inner junction [(b) $H=1.6H_0$], followed by junctions Nos. 2 and 4 [(c) $H=2.7H_0$].

should be noted that, since the total thickness of the stack is much smaller than the London penetration depth, only a tiny fraction of the external field actually is screened. At higher fields vortices start to penetrate the middle junction [Fig. 7(b)]. The other junctions stay free of vortices up to $2.5H_0$, when vortices start to penetrate junctions Nos. 2 and 4 [Fig. 7(c)], whereas junctions Nos. 1 and 5 are free of vortices up to $H_{ext} \approx 5H_0$. We note that, for a single junction, the threshold for flux entry is given by[7] $H_{thr} = \Phi_0/(\pi t_{eff} \mu_0 \lambda_j)$, which equals $5.8H_0$ for the junction parameters used.

We now turn to dynamic solutions. For $H_{ext}=0$, $j_{ext}>0$, there are zero-field modes very similar to the single-junction case (vortices moving back and forth) if we place one or several vortices into one junction. Their maximum speed depends slightly on the position of the junction within the stack. Vortices located in the outermost junctions move about 5% faster than vortices located in the middle junction.

Next, we investigated situations with several vortices placed into different junctions. If one vortex is placed into junction 1 and a second one into junction 5, we find that both the coherent (no phase shift between the vortices) and the symmetric (phase shift of $\pi$ between the vortices) modes are stable. This situation is very similar to the two-junction stack discussed in Ref. 6. If, on the other hand, one vortex is placed into junction 2 and a second one into junction 4, only the symmetric mode is stable. If vortices are placed into junctions Nos. 1, 3, and 5 or into all five junctions, the situation turns out to be unstable. In this case we found neither coherent nor symmetric modes. Typically, the stack returns either to one of the states discussed above or switches to a high-voltage state with complicated current distributions.

In magnetic fields which are not too large, we observe the Fiske modes known from single junctions if we place vortices into only one junction. If vortices are located in different junctions, very few simple modes like three vortices moving in the middle junction and one vortex moving in both adjacent junctions can be found; however, more complicated modes again turned out to be unstable. In contrast, strong phase locking occurs in the flux-flow regime (i.e., in large magnetic fields). Here vortex rows moving in one junction excite large standing waves in all junctions, which in turn triggers the vortex motion. A situation where vortices on all junctions move in phase is shown in Fig. 8. As will be discussed elsewhere,[16] in general we find situations where the amplitudes of standing waves vary sinusoidally also along the $z$ direction, the most stable situations being found for the complete symmetric mode as discussed above and the complete antisymmetric mode with a phase shift of $\pi$ between neighboring layers. Such resonances were found experimentally by Ustinov, Kohlstedt, and Heiden in long double junctions.[13]

In summary, the model predicts that zero-field and Fiske modes are only poorly developed in stacked Josephson junctions. In contrast, stable collective modes occur in the flux-flow regime. Here fluxons moving in different layers are triggered by standing waves excited in all junctions.

## III. SAMPLE CHARACTERIZATION AND MEASURING TECHNIQUES

The stacked Nb/Al-$AlO_x$/Nb tunnel junctions were fabricated on thermally oxidized silicon wafers. The Nb and Al layers were deposited using dc and rf magnetron sputtering, respectively. The bottom Nb layer is 100 nm thick, the following Nb layers have a thickness of 35 nm, and the upper Nb layer is 250 nm thick. The tunnel barriers were formed by thermal oxidation of 8-nm-thick Al layers in a pure oxygen atmosphere. The sample under discussion consists of $N=7$ Josephson junctions with a lateral dimension of $20\times20$ $\mu m^2$ (cf. Fig. 3). The critical current density at $T=4.2$ K is 250 A/cm$^2$. The average gap voltage $2\Delta$ at 4.2 K is 2.4 mV. Various junction parameters, as discussed in Sec. II, are listed in Table I.

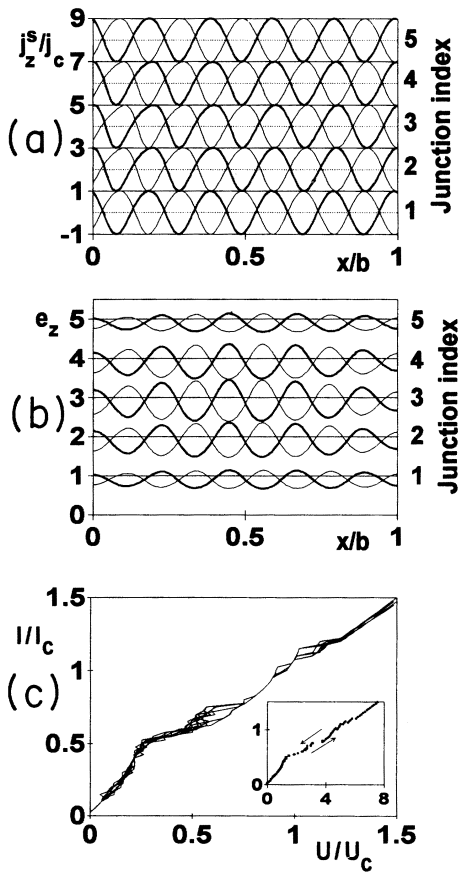


FIG. 8. Phase-locked state of a stack of five Josephson junctions ($j_{ext}=0.94j_c$, $H_{ext}=5H_0$, $\beta_c=20$). For the critical current densities, a spread of 5% has been assumed. (a) Josephson currents and (b) electric fields in units of $j_c\rho$ (offset of one per junction). Thick and thin lines in (a) and (b) correspond to a time difference of 3.5 in units of $\Phi_0/(2\pi j_c \rho t)$. (c) Superposition of the $I$-$V$ characteristics of the single junctions of the stack. In the phase-locked regions, the voltages across the junctions are equal. The inset shows the total $I$-$V$ characteristic, i.e., the bias current vs the sum of the average voltages of the five junctions.

TABLE I. Properties of Nb/Al-$AlO_x$/Nb and BSCCO multilayers. The Josephson plasma frequency is defined as $f_{pl}=[j_c t/(2\pi\Phi_0\epsilon\epsilon_0)]^{1/2}$ and the characteristic frequency $f_c=V_c/\Phi_0$.

| | Nb-Al-$AlO_x$-Nb | $Bi_2Sr_2CaCu_2O_{8+x}$ $(Pb_yBi_{1-y})_2Sr_2CaCu_2O_{8+x}$ |
|---|---|---|
| Electrode thickness (Å)[a] | 410 | 3 |
| Barrier thickness (Å) | 20 | 12 |
| Critical current density ($A/cm^2$) | 250 | 100–7000 |
| London penetration depth (Å) | 900 | 1700 |
| Magnetic length $\lambda_m$ ($\mu$m)[a] | 47 | 50–400 |
| Kinetic length $\lambda_k$ ($\mu$m)[a] | 23 | 0.2–1 |
| Characteristic voltage $V_c$ (mV)[b] | 2.6 | 0.2–15 |
| Characteristic frequency (GHz) | 1100 | 500–7000 |
| Plasma frequency (GHz) | 90 | 30–250 |

[a]For Nb-Al-$AlO_x$-Nb the values have been given for the inner Josephson junctions.
[b]For BSCCO we define $V_c$ as the voltage jump at $I_c$; for Nb-Al-$AlO_x$-Nb, $V_c=2\Delta/e$.

$Bi_2Sr_2CaCu_2O_{8+x}$ single crystals were grown from a stoichiometric mixture of the oxides and carbonates, heated up to 980 °C, and then cooled down to 800 °C at a rate of 1 °C/h. Composition and homogeneity of the crystals were checked by standard microprobe and x-ray analysis. Single crystals of the composition $(Bi_{1-y}Pb_y)_2Sr_2Cu_2O_{8+x}$ (PBSCCO), with lead contents $y$ up to 20%, have been grown by Régi *et al.*[14] For $c$-axis transport experiments, gold layers were evaporated on both faces of the crystals. The oxygen content of the crystals was varied by annealing in Ar or $O_2$. The sample dimensions in the $ab$ direction ranged between 20 and 100 $\mu$m and crystal thicknesses between 1 and 6 $\mu$m. The critical temperatures of the BSCCO single crystals, measured resistively, varied between 80 K for $O_2$-annealed samples and 90 K for Ar-annealed samples. The transition widths $\Delta T_c$ ranged between 0.5 and 3 K. $T_c$ of the PBSCCO crystals ranged between 55 and 92 K, depending on lead content and annealing condition. $\Delta T_c$ was similar to the BSCCO crystals. The critical current densities, measured resistively at $T=4.2$ K, depend strongly on annealing conditions. For Ar-annealed BSCCO, $j_c=100$ $A/cm^2$. Oxygen anneal as well as lead doping leads to an increase of $j_c$ up to 7000 $A/cm^2$ for $O_2$-annealed PBSCCO with 20% of Bi substituted by Pb.

Typical junction parameters, as calculated from the $I$-$V$ characteristics, are listed in Table I.

To perform the $c$-axis transport measurements, a two-terminal technique was used for BSCCO and PBSCCO. The crystals were mounted between two contact rods. The contact resistivity of the samples ranged between $10^{-6}$ and $10^{-4}$ $\Omega\,cm^2$, which yields ratios of $R_{contact}/R_{crystal}$ of less than 0.05 for our typical crystal dimensions of $30\times30$ $\mu m^2$ in the $a,b$ direction and 1 $\mu$m in the $c$ direction. In all figures shown below, the contact resistance is subtracted. Low-pass filters mounted in each current and voltage lead were used to shield external noise. For the magnetic field measurements, the crystals were oriented by a two-axis goniometer. The misalignment of the samples with respect to the external magnetic field direction was less than 0.5°.

## IV. RESULTS

### A. $I$-$V$ characteristics at zero magnetic field

#### 1. Nb/Al-$AlO_x$/Nb

As discussed in Sec. II, the Nb/Al-$AlO_x$/Nb samples can be regarded as stacks of small Josephson junctions; i.e., their lateral widths are smaller than $\lambda_j$. In the absence of an external magnetic field, the coupling terms in Eq. (4) are small; i.e., within our model we are dealing with a series connection of independent junctions. Since the $I$-$V$ characteristic of each junction consists of a zero-voltage branch for bias currents below the critical current $I_c$ and of a resistive branch for currents above the return current, $I_r<I_c$. For $I_r<I<I_c$ a plot of the total voltage across a stack of $N$ junctions vs bias current exhibits $N$ branches differing by the number of junctions in the resistive state. However, interactions between the different junctions may arise from quasiparticles generated in the resistive state. This leads to situations where at least some junctions of the stack can only simultaneously switch into the resistive state. Additionally, gap voltage and critical currents of the junctions may differ from the noninteracting case.

A typical $I$-$V$ characteristic of a stack of seven junctions in zero magnetic field is shown in Fig. 9. By ramping the bias current repeatedly up and down, it has been almost always possible to switch the junctions of the stack to their quasiparticle branch one by one, similar to the noninteracting case discussed above. However, if more than one junction is in the resistive state, the $I$-$V$ curve exhibits a negative slope at the gap voltage which rises with the number of junctions in the resistive state. For all junctions in the resistive state, the gap voltage is reduced between 3% at small bias currents and 16% at large bias currents.

This feature may partially be due to self-heating of the sample. In fact, at temperatures below the $\lambda$ point of liquid He the negative slope was reduced. Nevertheless, it did not disappear completely, indicating that a none-

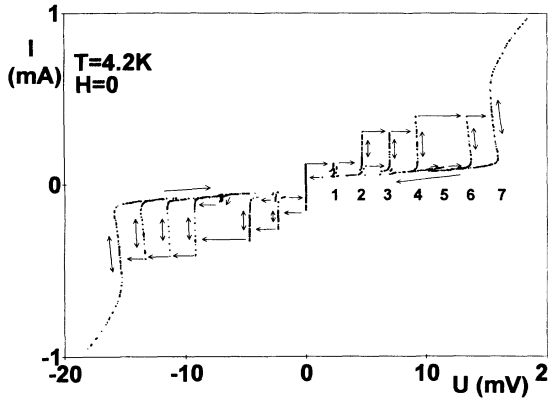


FIG. 9. *I-V* characteristic of the stack of seven Nb/Al-$AlO_x$/Nb junctions. The arrows indicate the direction of the current sweeps. The indices of the branches correspond to the number of junctions in the resistive state.

quilibrium injection of quasiparticles is in fact one of the important interaction mechanisms in these samples.

### 2. BSCCO

In contrast to the Nb/Al-$AlO_x$/Nb stacks, the BSCCO crystals are large compared to $\lambda_j$, but still small compared to $\lambda_m$. In this case model simulations show that for magnetic fields $H \ll H_0$ all junctions essentially act like independent short junctions. However, since the electrode thickness is only 3 Å, interactions via quasiparticle injection may be very strong. For Ar-annealed BSCCO crystals with critical current densities of typically 100 A/cm$^2$ at $T=4.2$ K, the *I-V* characteristics exhibit multiple branching very similar to the Nb/Al-$AlO_x$/Nb stacks, indicating that interactions between different junctions are small. Figure 10 shows an example for $T=4.2$ K. The crystal thickness is 1.8 $\mu$m; i.e., the sample consists of $N \approx 1200$ junctions. Except for two junctions having a critical current well below 1 mA, most of the junctions switch into the resistive state at bias currents between 1.5 and 2.5 mA. Just above the critical current of an individual junction, we observe an additional voltage drop of $V_c \approx 14$ mV, which is not too far below a hypothetical BCS value of the gap, $2\Delta = 3.5 k_B T_c \approx 21$ mV. At bias currents above 2.5 mA, all junctions have switched to the resistive state. The corresponding quasiparticle branch is nearly vertical. Assuming that the voltage drop of 4.1 V equals the sum of the gap voltages of all junctions, we calculate a gap voltage of 3.4 mV per junction, which is far below the BCS value of 21 mV. Since we have already observed a gap suppression of up to 16% in the Nb/Al-$AlO_x$Nb stacks, it seems natural that the large gap suppression observed in the very densely packed BSCCO junctions is also due to quasiparticle injection. If this mechanism is responsible for interactions between different junctions, it should be possible to increase the coupling strength by increasing the critical density of the Josephson currents.

In fact, we only observe simultaneous switching of all junctions in oxygen-annealed crystals of the composition $(Bi_{0.8}Pb_{0.2})_2Sr_2CaCu_2O_8$ (Fig. 11). For these crystals the critical current density at $T=4.2$ K is 7 kA/cm,$^2$ i.e., almost two orders of magnitude larger than for the Ar-annealed BSCCO crystals and the Nb/Al-$AlO_x$/Nb stacks. The *I-V* characteristic in Fig. 11 can be described well by a resistively shunted junction (RSJ) simulation using $\beta_c \approx 2.1$ and an $I_c R_N$ product of $\approx 60$ mV. Similar results have recently been obtained by Régi *et al.*, using a different measuring technique.[14] If we take the voltage jump above the critical current as the sum gap, we find a gap of less than 1 mV per junction, i.e., a factor of 3 smaller than in Ar-annealed BSCCO.

To conclude, in zero magnetic field both the Nb/Al-$AlO_x$/Nb stacks and the Ar-annealed BSCCO single crystals exhibit multiply branched *I-V* characteristics. Although a gap suppression is observed in both systems, the different junctions of the stacks are only weakly coupled. In contrast, the natural Josephson junctions in oxygen-annealed $(Bi_{0.8}Pb_{0.2})_2Sr_2CaCu_2O_8$ crystals switch simultaneously into the resistive state and seem to be rigidly coupled. This behavior is accompanied by a considerably reduced McCumber parameter $\beta_c$.

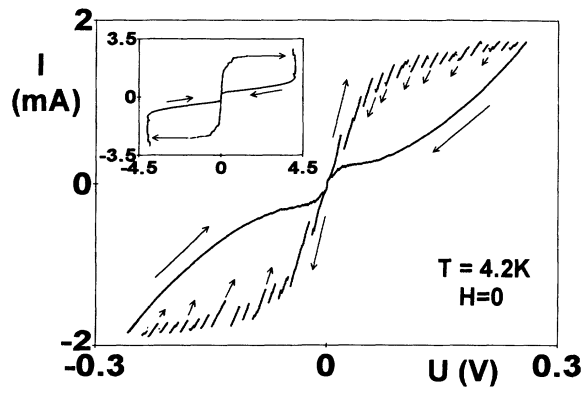


FIG. 10. *I-V* characteristic of a BSCCO single crystal (annealed in Ar) exhibiting a large number of quasiparticle branches. The critical current density was 140 A/cm.$^2$ The quasiparticle branches have not been traced out completely. The inset shows the *I-V* characteristic on a larger voltage scale.

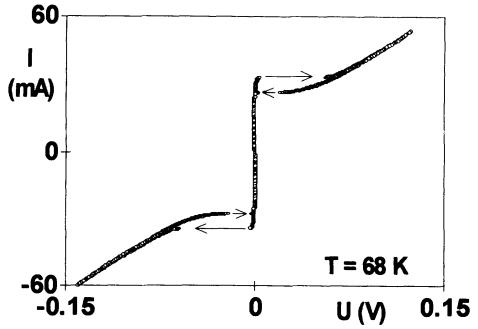


FIG. 11. *I-V* characteristic of a PBSCCO single crystal (annealed in $O_2$) exhibiting only a single resistive branch. The critical current density at 4.2 K was 7 kA/cm$^2$.

### B. Magnetic field dependence of the critical current

#### 1. *Nb/Al-AlO$_x$/Nb*

Since the Nb/Al-AlO$_x$/Nb multilayers can be regarded as stacks of short Josephson junctions, $I_c(H)$ of each junction should follow a Fraunhofer pattern. For the outer junctions, we expect the first zero of $I_c$ at $H_0=10$ and 14 Oe, respectively. For the inner junctions, $H_0=24$ Oe.

A typical measurement is shown in Fig. 12. The critical current of the first junction becoming resistive could be determined from a 5-$\mu$V voltage criterion. The critical currents of all other junctions have been defined as the currents at which switching to the quasiparticle branch occurs. For magnetic fields smaller than 2 Oe, we find that one junction becomes resistive at a bias current of 0.25 mA. Two junctions switch at $I\approx 0.34$ mA, and a group of three junctions switches at 0.43 mA, whereas the last junction becomes resistive at $I\approx 0.5$ mA. Increasing the magnetic field, the critical current of one junction from the three-junction group decreases strongly, reaching its first zero at $H=11$ Oe. The junction having the highest critical current in zero magnetic field reaches its first $I_c$ minimum at $H=13$ Oe. Up to $H=20$ Oe the critical current of all other junctions decrease monotonically to 40% of their zero-field values. At higher values of the magnetic field, the *I-V* curve is smeared out by flux flow, making it impossible to identify the critical currents of individual junctions. In certain regions of the magnetic field, we observe that the critical currents of different junctions "snap" together; i.e., they switch into the resistive state at the same current. In Fig. 12 some of these regions are highlighted by lines.

Figure 13 shows a model simulation where we used the geometry of the Nb/Al-AlO$_x$/Nb stack. The critical current densities have been chose such that the $I_c$ distribution as measured in zero magnetic field was reproduced. We find that, essentially, the critical current of

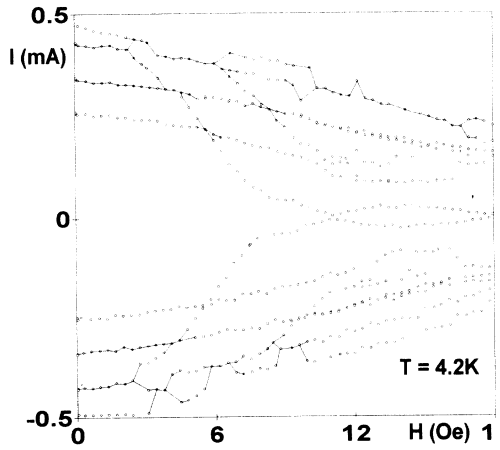


FIG. 12. Magnetic field dependence of the critical currents of the Nb/Al-AlO$_x$/Nb stack. The lines denote regions where phase locking occurs.

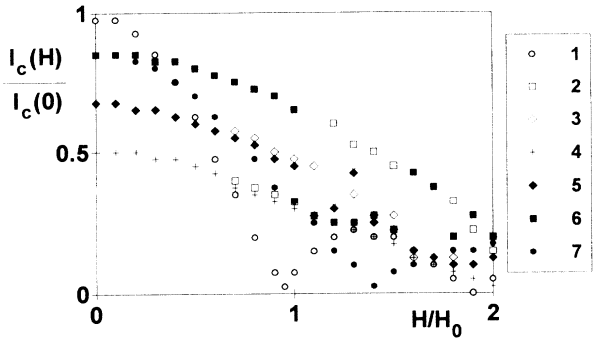


FIG. 13. Simulation of the $I_c(H)$ dependence of a stack of seven Josephson junctions. Junction parameters as measured for the Nb/Al-AlO$_x$Nb stack have been used.

each junction follows a Fraunhofer pattern with field scales $H_0$ as expected from the different effective junction thicknesses. Also here, at certain magnetic fields, some junctions switch together into the resistive state. However, the field range of collective switching is much smaller than in the experiment, again indicating that other coupling mechanisms, e.g., quasiparticle injection, are important for this geometry.

#### 2. *BSCCO*

We start by discussing the magnetic field dependence of the critical current and show typical *I-V* characteristics recorded in magnetic fields up to 1 kOe (Fig. 14). The most prominent feature is the appearance of approximately linear, nonhysteretic sections before switching to the next quasiparticle branch occurs [Fig. 14(b)]. Within these sections there are voltage jumps of typically 100 $\mu$V. Additionally, irregular spaced "steps" with a reduced differential resistance can be observed. As supported from our model calculations, these regions may result from a superposition of different Fiske steps of several junctions. In large magnetic fields [Fig. 14(c)], the linear sections split into several hysteretic branches with voltage spacings of typically 0.5 mV. In this region we possibly observe the collective flux-flow modes as predicted from our model (Fig. 8). This observation is supported by *X*-band microwave emission experiments.[15] There we found that the emitted microwave power increased strongly with increasing magnetic field.

A typical $I_c(H)$ pattern, as derived from the voltage jumps in the *I-V* characteristics, is shown in Fig. 15. There is a monotonic decrease of all critical currents for fields up to $H\approx H_0$. At higher fields the critical currents of almost all junctions saturate between 60% and 80% of their zero-field values, exhibiting shallow local maxima and minima. Measuring crystals with lateral dimensions between 20 and 80 $\mu$m, we find that the first $I_c$ minimum is proportional to the inverse crystal width $b$, the slope being determined by

$$H_0=\frac{\Phi_0}{\mu_0 b(15\ \text{Å})},$$

as expected for the intrinsic Josephson junctions in BSCCO (Fig. 15, inset).

Figure 16 shows the magnetic field dependence of several critical currents of one single crystal. Within some finite magnetic field ranges, we observe that, similar to the Nb/Al-$AlO_x$/Nb stacks, several junctions of the stack switch into the resistive state simultaneously. The quasiparticle branches of these junctions can still be traced out, but only by starting from a branch located at high voltages, decreasing the bias current below the return current and increasing it again [see arrows in Fig. 14(b)].

The essential features of the measured $I_c(H)$—a first decrease of the critical current in fields up to $H_0$ followed by shallow modulations—are qualitatively reproduced in model calculations for a stack of five junctions, where we used the same junction parameters as for the simulations discussed in Sec. II (Fig. 17). For $H > H_0$, $I_c$ of the inner junction decreases strongly, whereas the critical currents of all other junctions stay flat up to $2H_0$, where the $I_c$'s of junctions Nos. 2 and 4 start to decrease strongly. The figure also shows that the critical currents of different

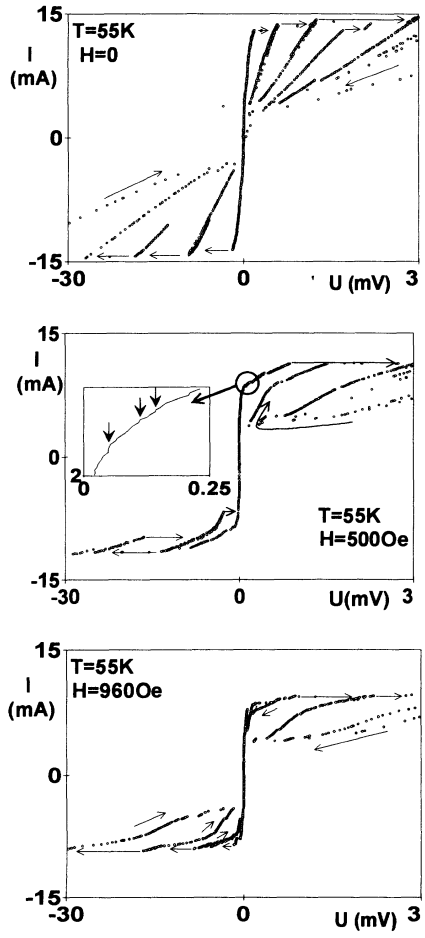


FIG. 14. *I-V* characteristics of a BSCCO single crystal at three different magnetic fields. The inset in the middle part of the figure shows an enlarged part of the curve. Fiske steps can clearly be seen.

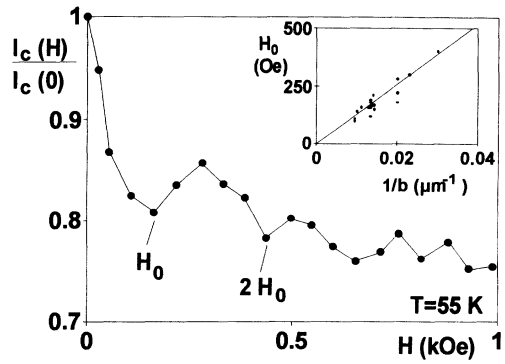


FIG. 15. Magnetic field dependence of the $I_c$ of the lowest branch of an intrinsic Josephson junction in BSCCO. The inset shows the first $I_c$ minimum vs crystal width for several single crystals. The solid line corresponds to $H_0 = \Phi_0/[\mu_0 b\,(15\ \text{Å})]$.

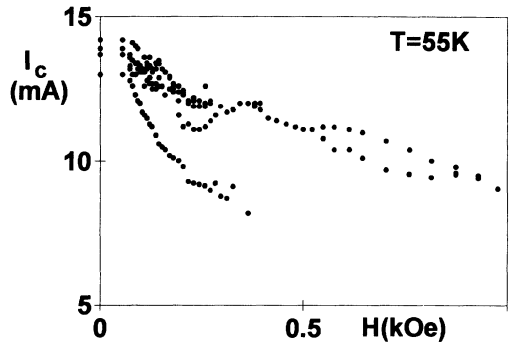


FIG. 16. $I_c$ vs $H$ of the first four branches of one BSCCO single crystal. Around $H = 0.5$ kOe, simultaneous switching of several junctions is observed.

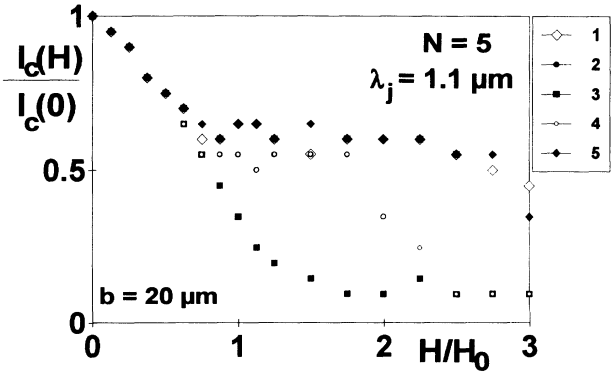


FIG. 17. Simulation of $I_c(H)$ of the five Josephson junctions, labeled 1–5, in a stack of $N = 5$. For the simulation typical BSCCO parameters have been used.

junctions "snaps" together in certain ranges of the magnetic field very similar to the experimental observations in the Nb/Al-$AlO_x$Nb stacks.

## V. CONCLUSIONS

In summary, we have compared two different types of stacked Josephson junction structures, Nb/Al-$AlO_x$/Nb, multilayers and natural Josephson junctions in $(Bi_{1-y}Pb_y)_2Sr_2CaCu_2O_{8+x}$ single crystals. The Nb/Al-$AlO_x$/Nb multilayers and the BSCCO single crystals with low critical current density exhibit multiple branched *I-V* characteristics in zero magnetic field, indicating that the interaction between different junctions is small. In contrast, collective switching of all junctions of the stack has been observed in BSCCO single crystals with high critical current density. For finite magnetic fields, both experiments and simulations indicate that coupling via currents flowing along the superconducting layers is essential. Model simulations predict that a large number of junctions can be phase locked in the flux-flow regime at sufficiently high magnetic fields.

## ACKNOWLEDGMENTS

The authors wish to thank A. V. Ustinov for valuable suggestions, P. Bodin for demonstration programs, and P. Pospischil and C. Kreuzer for several measurements. Financial support by the Bayerische Forschungsstiftung via the FORSUPRA consortium and by the Bundesministerium für Forschung und Technologie via the Josephson array consortium is gratefully acknowledged.

[1] *Superconducting Devices*, edited by S. T. Ruggiero and D. A. Rudman (Academic, New York, 1990).

[2] R. Pöpel, J. Niemeyer, R. Fromknecht, W. Meyer, and L. Grimm, J. Appl. Pys. **68**, 4294 (1990); C. A. Hamilton, C. Burroughs, and K. Chieh, J. Res. Natl. Inst. Stand. Technol. **95**, 219 (1990); J. A. Stern, H. G. LeDuc, and J. Zmuidszinas, IEEE Trans. Appl. Supercond. **AS-3**, 2485 (1993).

[3] A. K. Jain, K. K. Likharev, J. E. Lukens, and J. E. Sauvageau, Phys. Rep. **109**, 311 (1984).

[4] H. Kohlstedt, G. Hallmanns, F. P. Nevirkovets, D. Guggi, and C. Heiden, IEEE Trans. Appl. Supercond. **AS-3**, 2197 (1993); I. P. Nevirkovets, H. Kohlstedt, G. Hallmanns, and C. Heiden, Supercond. Sci. Technol. **6**, 146 (1993).

[5] R. Kleiner, F. Steinmeyer, G. Kunkel, and P. Müller, Phys. Rev. Lett. **68**, 2394 (1992); R. Kleiner and P. Müller, Phys. Rev. B **49**, 1327 (1994); R. Kleiner, F. Steinmeyer, G. Kunkel, and P. Müller, Physica C **185-189**, 2617 (1991); B. Aigner, B. Avenhaus, R. Kleiner, C. Kreuzer, G. Kunkel, P. Pospischil, F. Steinmeyer, P. Müller, and K. Andres, IEEE Trans. Appl. Supercond. **3**, 2281 (1993); R. Kleiner, B. Aigner, B. Avenhaus, C. Kreuzer, P. Pospischil, F. Steinmeyer, P. Müller, and K. Andres, Physica B **194-196**, 1753 (1994).

[6] S. Sakai, P. Bodin, and N. F. Pedersen, J. Appl. Phys. **73**, 2411 (1993).

[7] R. D. Parmentier, in *The New Superconducting Electronics*, edited by H. Weinstock and R. W. Ralston (Kluwer, Dordrecht, 1993).

[8] H. Amin, M. G. Blamire, and J. E. Evetts, IEEE Trans. Appl. Supercond. **AS-3**, 2204 (1993).

[9] A. V. Ustinov, H. Kohlstedt, M. Cirillo, N. F. Pedersen, G. Hallmanns, and C. Heiden, Phys. Rev. B **48**, 10 614 (1993); N. Grønbech-Jensen and J. A. Blackburn, Phys. Rev. Lett. **70**, 1251 (1993); D. Winkler, Physica B **194-196**, 1771 (1994).

[10] K. Enpuku, K. Yoshida, and F. Irie, J. Appl. Phys. **52**, 344 (1981); S. Pagano, M. P. Soergensen, R. D. Parmentier, P. L. Christiansen, and O. Skovgaard, Phys. Rev. B **33**, 174 (1986); G. Rotoli, G. Costabile, and R. D. Parmentier, *ibid.* **41**, 1958 (1990).

[11] J. R. Clem and M. W. Coffey, Phys. Rev. B **42**, 6209 (1990).

[12] L. Bulaevskii and J. R. Clem, Phys. Rev. B **44**, 10 234 (1991).

[13] A. V. Ustinov, H. Kohlstedt, and C. Heiden (unpublished).

[14] F. X. Régi, J. Schneck, H. Savary, C. Daguet, and F. Huet, IEEE Trans. Appl. Supercond. **3**, 1190 (1993); F. X. Régi, J. Schneck, H. Savary, H. Mellet, P. Müller, and R. Kleiner, J. Phys. (Paris) (to be published); F. X. Régi, J. Schneck, J. F. Palmier, and H. Savary (unpublished).

[15] G. Hechtfischer, R. Kleiner, and P. Müller (unpublished).

[16] R. Kleiner (unpublished).

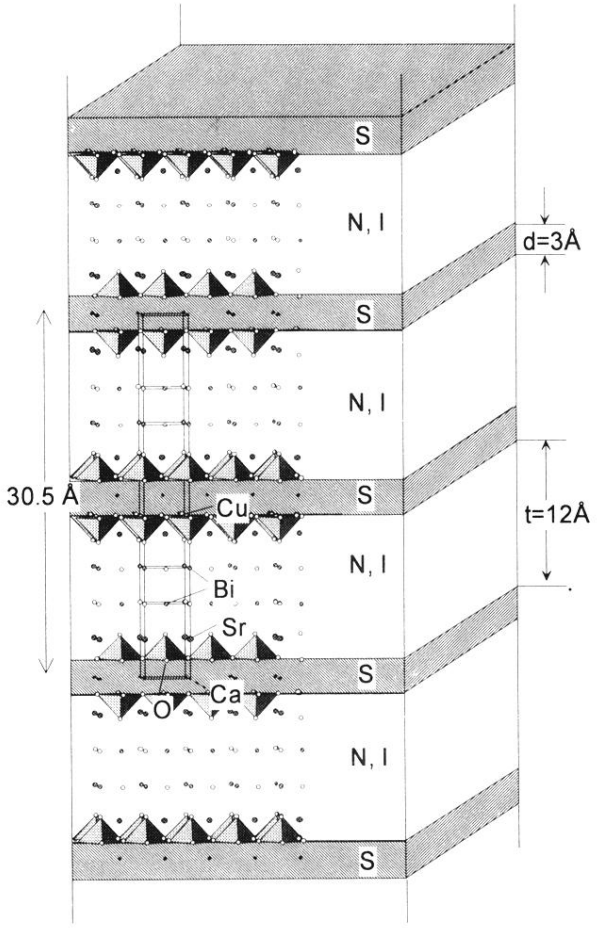


FIG. 1. Superposition of the crystal structure of BSCCO and the model of stacked intrinsic Josephson junctions. *S*, superconducting $CuO_2$ bilayer; *N*,*I*, normal or insulating layer consisting of $Bi_2O_3$ and SrO.

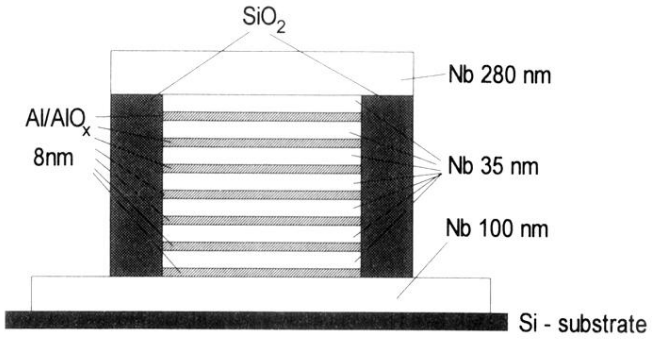


**FIG. 3. Schematic view of the stack of seven Nb/Al-$AlO_x$/Nb junctions.**